Catalysis Letters (2022) 152:2738–2744
https://doi.org/10.1007/s10562-021-03850-y

Ni-Foam Structured Ni-Phyllosilicate Ensemble as an Efficient Monolithic Catalyst for CO_2 Methanation

Yaqi Chen[1] · Xiaoren Wu[2] · Qing Liu[1] · Maoshuai He[3] · Hongcun Bai[4]

Received: 14 September 2021 / Accepted: 27 October 2021 / Published online: 9 November 2021

Abstract

This work proposed a new path to synthesize Ni-phyllosilicate through the reaction of nickel hydroxide and silica sol on the surface of Ni-foam to form the monolithic Ni-phyllosilicate/Ni-foam catalyst. Ni-phyllosilicate could reprint the morphology of nickel hydroxid and firmly anchor on the framework of Ni-foam, which obtained fine Ni particles of 2.8 nm after reduction in H_2 at 650 °C, resulting in high catalytic activity for CO_2 methanation. In addition, the Ni-phyllosilicate/Ni-foam catalyst showed high long-term stability in a 100 h-lifetime test owing to the combined effects of surface confinement of Ni-phyllosilicate, firm anchoring between Ni-phyllosilicate and Ni-foam, as well as the high heat transfer property of Ni-foam.

Graphical Abstract

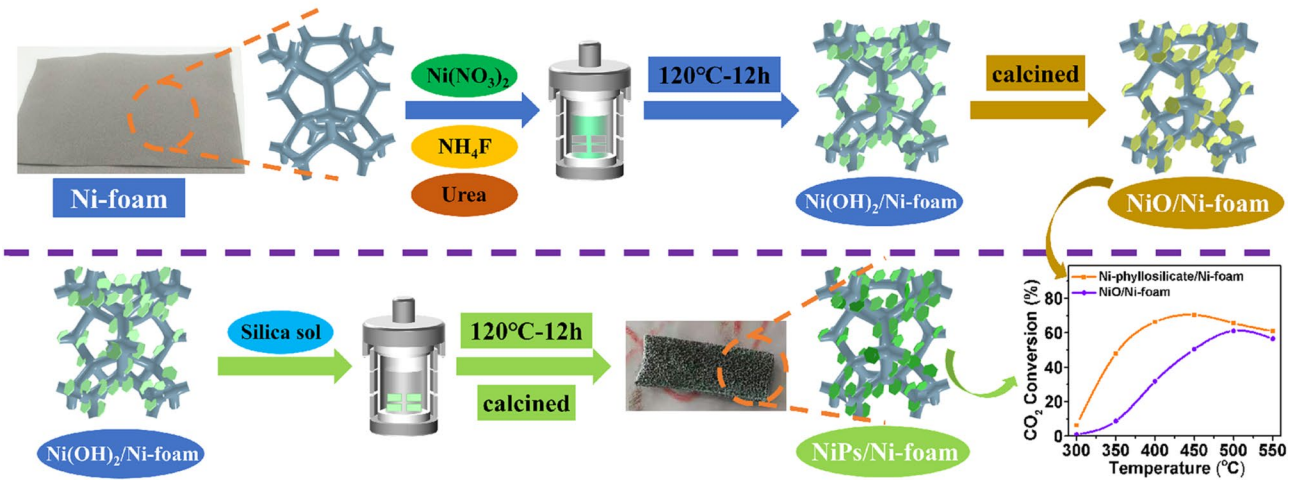

Keywords Ni-phyllosilicate · Nickel hydroxide · Ni-foam · Sacrificial template · Monolithic catalyst

✉ Qing Liu
qliu@sdust.edu.cn

✉ Maoshuai He
hemaoshuai@qust.edu.cn

✉ Hongcun Bai
hongcunbai@nxu.edu.cn

[1] Key Laboratory of Low Carbon Energy and Chemical Engineering, Shandong University of Science and Technology, Qingdao 266590, China

[2] Schneider Electric (China) Co., Ltd., Beijing 100102, China

[3] Shandong Key Laboratory of Biochemical Analysis, College of Chemistry and Molecular Engineering, Qingdao University of Science and Technology, Qingdao 266042, China

[4] State Key Laboratory of High-efficiency Utilization of Coal and Green Chemical Engineering, Ningxia University, Yinchuan 750021, China

1 Introduction

Effective utilization of CO_2 is an important way to alleviate greenhouse effect and solve environmental problems [1]. As an abundant carbon resource, CO_2 can be converted to different fuels or chemicals including methanol, ethanol, gasoline, carbonates, urea, etc. Among them, the reaction of the captured CO_2 in industrial and renewable hydrogen to produce CH_4 in the presence of a catalyst, namely CO_2 methanation reaction, is an implementable route. At present, the Ni/SiO_2 catalysts [2, 3] have been used in CO_2 methanation with well catalytic performance. However, the CO_2 methanation is a typical exothermic reaction ($CO_2 + 4H_2 \rightarrow CH_4 + 2H_2O$, $\Delta H = -165.0$ kJ mol^{-1}), the poor thermal conductivity of silica support easily results in decrease of activity and even sintering deactivation [4]. Therefore, it is urgent to prepare a Ni/SiO_2 catalyst with good catalytic performance and anti-sintering property.

For the traditional powder Ni-based catalyst, molding treatment is necessary to form the catalyst with a certain shape, size, and strength. However, the availability of surface area usually decreases due to the high pressure during the molding process, which is adverse to mass transfer resulting in decline of catalytic activity. In other words, for the catalyst molding treatment, the mechanical strength and catalytic performance are contradictory. The metal-foams have been widely used in battery material and structured catalyst [5, 6], which has a small pressure drop, controllable mass transport, good thermal and mechanical properties, easy catalyst separation and recyclability, which make them superior to conventional catalysts [7]. For example, the foam-structured catalyst has achieved high catalytic performance for catalytic oxy-methane reforming reaction [8]. In addition, the free-standing $Ni-Al_2O_3$ ensemble derived from NiAl-layered double hydroxides (NiAl-LDHs) grown onto a Ni-foam, has cleverly realized high activity/selectivity and enhanced heat/mass transfer, which achieved remarkable results in the reaction of acetone hydrogenation to isopropanol [9]. In addition, $Ni(OH)_2$ has been regarded as the most promising electrode material due to its low cost, ultra-high specific capacitance and environmental friendliness. Moreover, many efforts have been put into growing $Ni(OH)_2$ onto three-dimensional porous Ni foam as binder-free electrodes for electrochemical energy storage applications [10–12]. Thus, constructing a metal-foam based monolithic catalyst with high activity, distinguished robustness and high stability is attractive.

Ni/SiO_2 catalysts can be obtained after reduction of Ni-phyllosilicate, which obtains strong metal-support interaction to overcome the Ni sintering on the silica support [13–15]. In general, Ni-phyllosilicate can be synthesized by hydrothermal method or ammonia evaporation method through the reaction of silicon precursors (such as sodium silicate [16], silica sol [17], and tetraethyl orthosilicate [18]) and soluble nickel slats (such as nickel nitrate [14], nickel chloride [16], nickel acetate [19], Ni acetylacetonate [19]) [20, 21]. As far as we know, there is no research on preparation of Ni-phyllosilicate using nickel hydroxide as sacrificial template. Therefore, it is interesting to study the feasibility of Ni-phyllosilicate formation through the interaction of nickel hydroxide and silica sol on the Ni-foam.

Herein, a monolithic Ni-phyllosilicate/Ni-foam catalyst was prepared using nickel hydroxide grown on the surface of Ni-foam as the sacrificial template through a simple two-step hydrothermal method for CO_2 methanation. It provides a unique combination of anti-sintering Ni-phyllosilicate as the active component and high permeability and enhanced mass/heat transfer stemmed from Ni-foam.

2 Experimental Section

2.1 Catalyst Preparation

The Ni-phyllosilicate/Ni-foam catalyst was prepared via growing Ni-phyllosilicate onto the monolithic Ni-foam substrate using a hydrothermal synthesis method. Typically, square Ni-foam chips (20 mm length, 10 mm width, 1 mm thickness, and 110 pores per inch; Kunshan GuangJiaYuan new materials Co., Ltd.) were soaked into concentrated HCl solution for a 10 min ultrasonic treatment to remove nickel oxide on the Ni-foam surface, and then, the chips were washed thoroughly by deionized water and ethanol.

The as-cleaned Ni-foam (0.550 g, 8 chips, 1*10*20 mm) were transferred into an autoclave (100 mL) filled with 50 mL of aqueous solution containing NH_4F (10 mmol), urea (12.5 mmol), and $Ni(NO_3)_2{\cdot}6H_2O$ (2 mmol), and subsequently hydrothermally treated at 120 °C for 12 h, and then the chips were rinsed with deionized water and ethanol to obtain the intermediate product $Ni(OH)_2$/Ni-foam.

NiO/Ni-foam could be obtained after calcination of $Ni(OH)_2$/Ni-foam at 400 °C for 4 h in the air.

Furthermore, $Ni(OH)_2$/Ni-foam (8 chips, 1*10*20 mm was transferred to an autoclave filled with 50 mL of deionized water and silica sol (silica, 6 mmol) for hydrothermal treatment at 120 °C for 12 h. After separation and calcination at 400 °C for 4 h, NiPs/Ni-foam was obtained, in which "NiPs" was abbreviation of "Ni-phyllosilicates".

2.2 Catalyst Characterizations and Catalytic Tests

The detailed operation procedures of catalyst characterizations and catalytic performances evaluations were displayed in Supporting Information Summary.

3 Results and Discussion

3.1 Morphology and Structure Characterizations

Ni-foam has the flexibility in tailoring the shape and size, and irregular three-dimensional void patterns (Fig. 1a), whose framework obtains a smooth surface (Fig. 1b) [9]. For NiO/Ni-foam, the sample shows a well-preserved monolith geometry with a Ni component attached to the surface of Ni-foam (Fig. 1c). What's more, the SEM image of NiO/Ni-foam clearly exhibits the hexagonal nano-sheet with thickness of 0.26 nm growing on the surface of Ni-foam (Fig. 1d). In addition, after the further hydrothermal treatment in the presence of silica sol, the surface of Ni-foam still retains the morphology and structure of nano-sheet (Fig. 1e and f), whose thickness decreases from 0.26 nm (Fig. 1d) to 0.18 μm (Fig. 1f). This result indicates that the obtained nano-sheet has strong interaction with Ni-foam, and the second hydrothermal treatment cannot destroy its structural characteristics.

XRD analyses were carried out on the as-cleaned Ni-foam, as-synthesized NiO/Ni-foam and NiPs/Ni-Foam; however, only obvious diffraction peaks ascribing to metallic Ni could be observed due to the too strong peak intensity of Ni-foam and relatively low loading amount of NiO or Ni-phyllosilicate (Fig. S1). Therefore, in order to avoid the interference of Ni-foam framework and identify the crystal information of the loaded species correctly, the nanosheets grown on the Ni-foam were scraped off for XRD analysis. For the $Ni(OH)_2$/Ni-foam, the diffraction peaks at 19.3, 33.5, 38.8, 52.3, 59.8 and 70.7° correspond to the (001), (100), (101), (102), (003) and (103) planes of $Ni(OH)_2$ (JCPDS No. 03-0177) [22, 23]. In addition, a small amount of $Ni(NO_3)_2(OH)_4$ can also be observed (JCPDS No. 22-0752) [24]. After calcination of $Ni(OH)_2$/Ni-foam, as shown in Fig. 2b, five diffraction peaks at 37.1, 43.2, 62.7, 75.3 and 79.3° are observed on the as-synthesized NiO/Ni-foam, which correspond to (111), (200), (220), (311) and (222) planes of NiO (JCPDS No. 47-1049) [25]. Obviously, no NiO diffraction peak is observed on the XRD pattern of NiPs/Ni-foam catalyst prepared by two-step hydrothermal process, and those at 19.5, 24.4, 34.1, 36.7 and 60.5° belonging to the planes (111), (004), (200), (202) and (060) of $Ni_3Si_2O_5(OH)_4$ (JCPDS No. 49-1859) can be observed (Fig. 2c) [26]. Here, it can be concluded that $Ni(OH)_2$ and $Ni_3(NO_3)_2(OH)_4$ not only provide the nickel species as the precursor, but also reprint their nanoflake morphology as the sacrificial template to form nickel phyllosilicate.

Moreover, the morphology information of the reduced catalyst and the dispersion of metallic nickel is obtained by TEM observation (Fig. 2d and e). For the 650 °C-redued NiO/Ni-foam, the metallic Ni particles are dispersed on the nanosheets, whose mean particle size reaches as large as 17.7 nm (Fig. 2d, Table 1), exhibiting a very poor Ni dispersion. Compared with NiO/Ni-foam, some wafer-thin nanosheets with many fine dark spots can be clearly seen on the reduced NiPs/Ni-foam (Fig. 2e), indicating that the characteristic nano-sheet structure can be remained after the reduction at high temperature [27]. In addition, its Ni particle size is only 2.8 nm (Table 1), exhibiting excellent

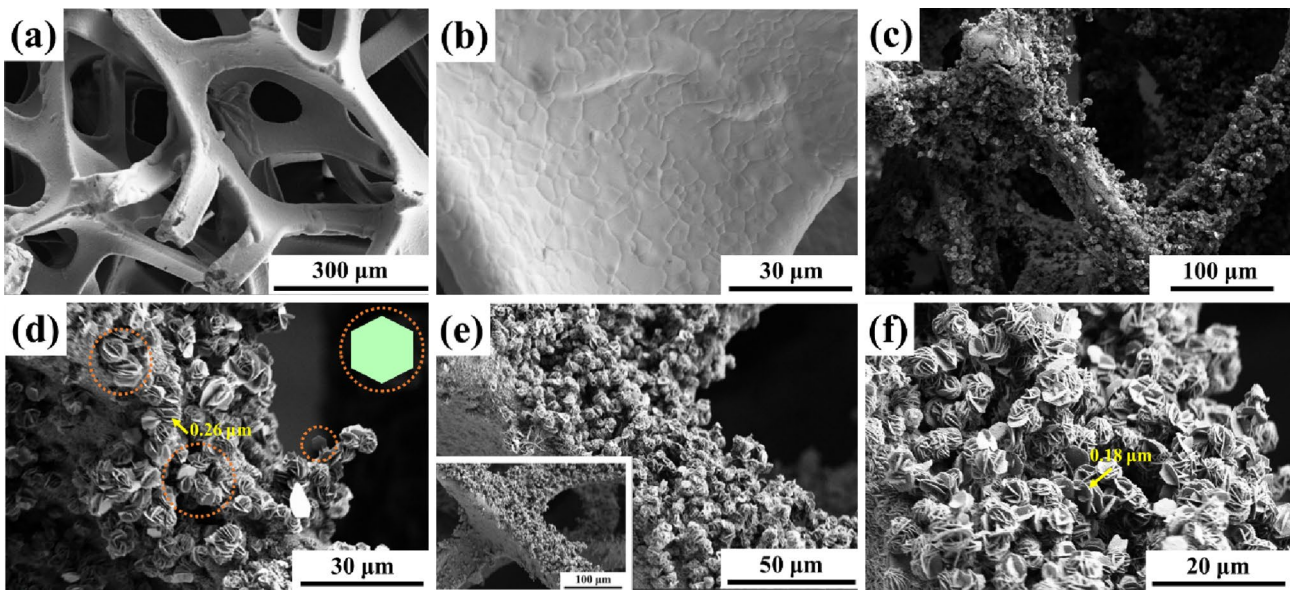

Fig. 1 SEM image of the pristine Ni-foam substrate (**a** and **b**), SEM images of the as-synthesized catalysts: (**c** and **d**) NiO/Ni-foam, (**e** and **f**) NiPs/Ni-foam

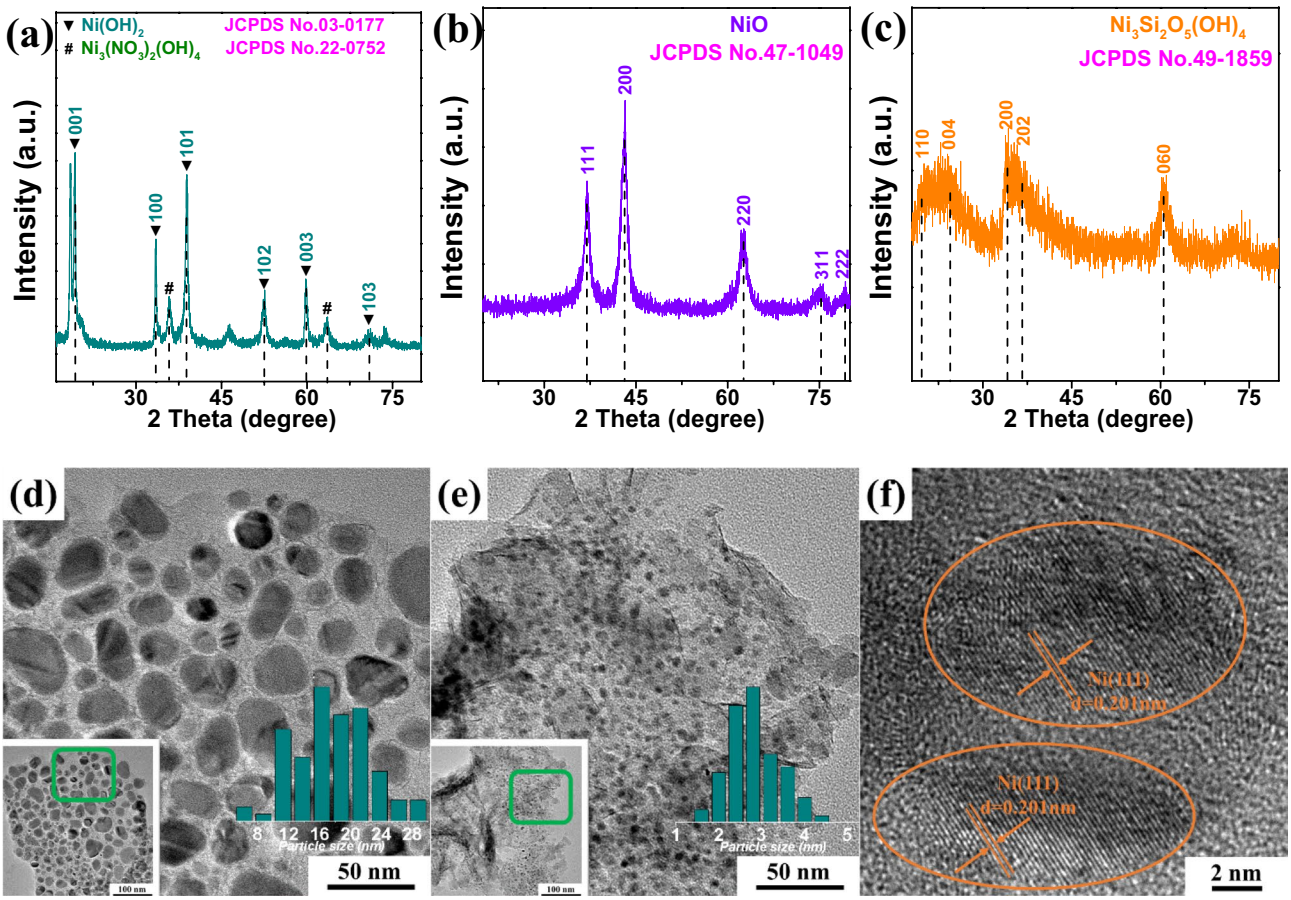

Fig. 2 XRD patterns of the as-synthesized catalysts and TEM images of the reduced catalysts: (**a**) $Ni(OH)_2$/Ni-foam, (**b** and **d**) NiO/Ni-foam, (**c** and **e**) NiPs/Ni-foam; and HRTEM image of the NiPs/Ni-foam (**f**). The scraped nickel-based species rather than the integral Ni-foam-based materials were analyzed by XRD and TEM

Table 1 Comparison of activities of different catalysts for CO_2 methanation

Catalyst	Ni particle size (nm)[a]	CO_2 conversion (%)	Temperature (°C)	Refs.
NiPs/Ni-foam	2.8	70.4	450	This work
NiO/Ni-foam	17.7	61.1	500	This work
$2Y_2O_3$-Ni/MgO-MCM-41	15.5[b]	~ 65.0	400	[34]
N_{180}/SR-U-24	5.25	~ 68.0	450	[2]
5% Ni/Al_2O_3	12.0	~ 63.0	440	[35]
$Ni/15Ce/Al_2O_3$	21.4	~ 63.0	450	[36]

[a]Estimated from the TEM images

[b]The particle size belongs to NiO

metal dispersion and anti-sintering property. Moreover, lattice spacing about 0.201 nm belong to the (111) crystal planes of Ni, which is consistent with the reported active center for CO_2 methanation (Fig. 2f) [28].

Combined with the above results, the formation process of the NiO/Ni-foam and NiPs/Ni-foam catalysts are described in Scheme 1. After the hydrothermal reaction of $Ni(NO_3)_2$, NH_4F and urea over Ni-foam at 120 °C for 12 h, $Ni(OH)_2$ and $Ni_3(NO_3)_2(OH)_4$ nanosheets grow on the surface of Ni-foam, and NiO/Ni-foam catalyst can be obtained after calcination. For NiPs/Ni-foam, nickel hydroxide reacted with silica sol to form Ni-phyllosilicate on the Ni-foam through a second hydrothermal reaction. As reported in literature [20, 29, 30], Ni-phyllosilicate is usually obtained through the reaction of silica and soluble nickel slat using hydrothermal method or ammonia evaporation method, in which silica plays a role of sacrifice template. In this work, it is found for the first time that Ni-phyllosilicate can be synthesized through the reaction of nickel hydroxide and silica sol, and the free-standing nickel hydroxide nanosheets on Ni-foam can be a novel sacrificial template to prepare Ni-phyllosilicate.

Scheme 1 Formation process of $Ni(OH)_2$/Ni-foam, NiO/Ni-foam and NiPs/Ni-foam

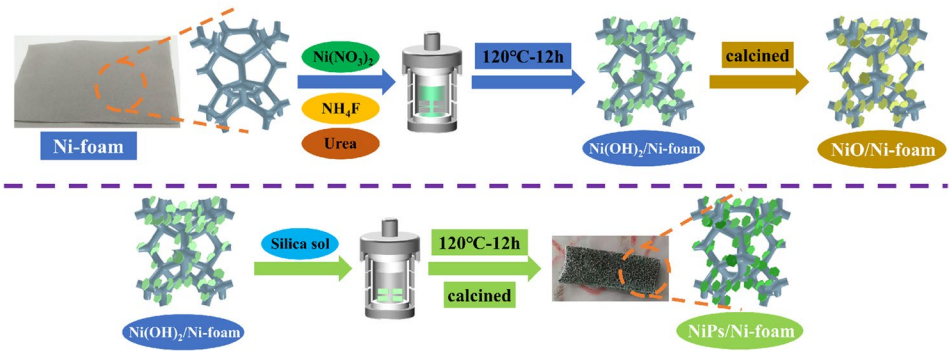

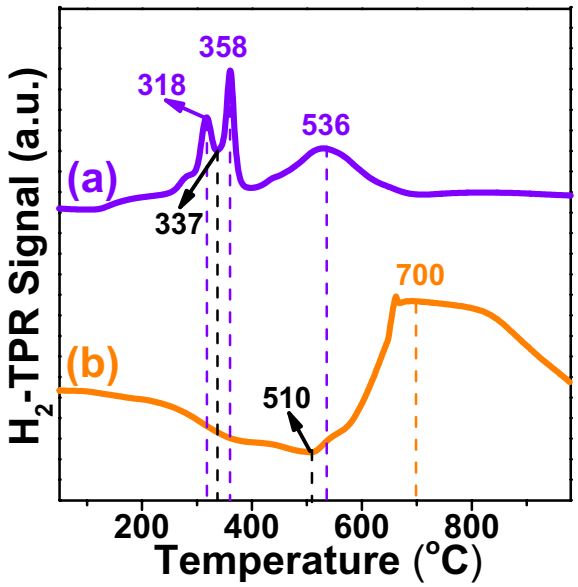

Fig. 3 H_2-TPR profiles: (a) NiO/Ni-foam and (b) NiPs/Ni-foam

3.2 Metal-Support Interaction Analysis

In Fig. 3, the H_2 consumption peaks at 318, 358 and 536 °C occur on the H_2-TPR profile of NiO/Ni-foam, attributing to the generated NiO with different interactions with Ni-foam framework. On the contrary, NiPs/Ni-foam catalyst only shows a strong H_2 consumption peak at the high temperature of 700 °C, indicating that Ni-phyllosilicate obtains strong metal-support interaction and nickel species can be reduced at a high temperature [3, 31]. In addition, there is the presence of another negative peak at around 510 °C over NiPs/Ni-foam, which may be attributed to the desorption of chemisorbed hydrogen on Ni-foam and the spillover hydrogen [32]. Moreover, for overall consideration, the reduction temperature of the catalysts were set at 650 °C for 1 h.

3.3 Effect of Active Components on Catalytic Activity

As shown in Fig. 4, the activities of thermodynamic equilibrium for CO_2 methanation show adverse effect with the operation temperature as a result of its strong exothermic

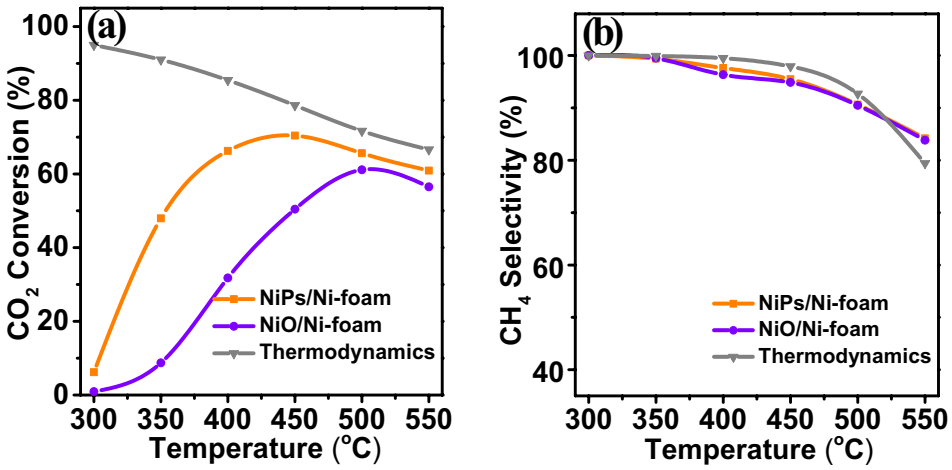

Fig. 4 Catalyst activity at 0.1 MPa: **a** CO_2 conversion and **b** CH_4 selectivity

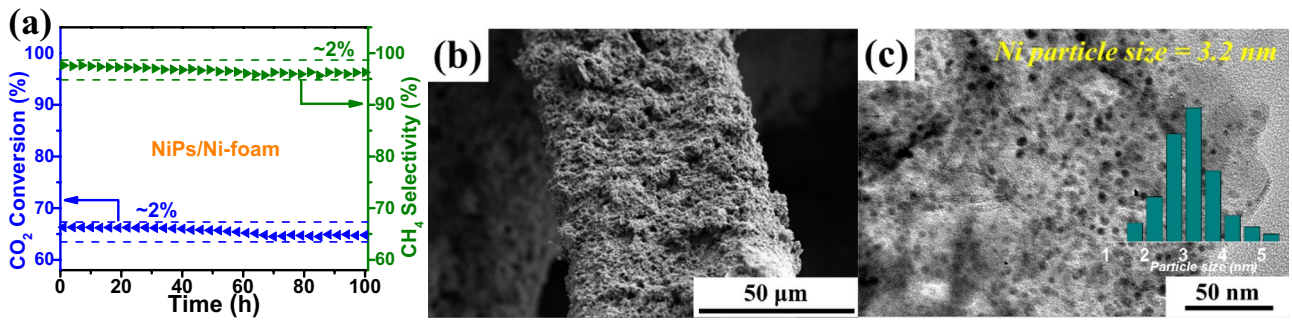

Fig. 5 Long-term stability test of the NiPs/Ni-foam catalyst: **a** catalytic activity at 400 °C, 0.1 MPa; **b** SEM images of the spent catalyst; **c** TEM images of the spent catalyst

property. The NiO/Ni-foam reaches the optimal catalytic activity at 500 °C, whose CO_2 conversion and CH_4 yield is 61.1% and 90.7%, respectively. On the contrary, the NiPs/Ni-foam achieves the optimal catalytic activity at 450 °C with CO_2 conversion of 70.4% and CH_4 yield of 95.5%. This is because the formation of small Ni particle size derived from the strong metal-support interaction of Ni-phyllosilicate over NiPs/Ni-foam. Besides, CO is the only by-product originated from the reverse water–gas shift or Boudouard reaction [33]. On the other hand, as shown in Fig. S2, in the low temperature reaction range of 200–300 °C, the catalysts CO_2 conversion was below 5%, effectively avoiding the occurrence of reverse reaction, and both catalysts have nearly 100% CH_4 selectivity. However, the NiPs/Ni-foam catalyst reached the activation temperature of the catalyst from about 225 °C, while NiO/Ni-foam catalyst began to show weak activity data at about 275 °C. In addition, as shown in Table 1, the reported $2Y_2O_3$-Ni/MgO-MCM-41 [34], N_{180}/SR-U-24 [2], 5% Ni/Al_2O_3 [35], and Ni/15Ce/Al_2O_3 [36] catalysts are compared as reference catalysts, the NiPs/Ni-foam catalyst exhibits the smallest Ni particle size and the highest CO_2 conversion, indicating that it is a competitive catalyst for CO_2 methanation.

3.4 Long-Term Stability Test

In order to investigate the long-term stability of the NiPs/Ni-foam catalyst, the 100 h-test was carried out at 400 °C, 0.1 MPa. It can be seen that the NiPs/Ni-foam exhibits high long-term stability, and the CO_2 conversion and CH_4 selectivity decrease by about 2% in the 100-h long-term test (Fig. 5a). After the long-term stability test, the spent NiPs/Ni-foam sample was recovered and characterized by SEM and TEM. Nanosheets can also be clearly observed on the spent NiPs/Ni-foam, indicating the strong interaction of NiPs and Ni-foam (Fig. 5b). On the other hand, for TEM, the Ni particles almost remain their original size with slight increase from 2.8 to 3.2 nm (Fig. 5c). Therefore, NiPs/Ni-foam is a promising monolithic catalyst with highly long-term stability. The contributions to high stability can be concluded as below: (1) The nanoflakes are firmly anchored on the surface of Ni-foam, which provides the structural stability of NiPs/Ni-foam; (2) The strong metal-support interaction of NiPs can construct confinement of Ni particles during the reduction and reaction processes, which provides its excellent anti-sintering property; (3) The high heat transfer property of Ni-foam can inhibit the occurrence of hotspots, which provides the excellent heat removal during the CO_2 methanation reaction process over NiPs/Ni-foam.

4 Conclusion

Nickel hydroxide was formed on the surface of Ni-foam to construct $Ni(OH)_2$/Ni-foam using hydrothermal treatment, which could be the sacrificial template and precursor to synthesize Ni-phyllosilicate using hydrothermal method to obtain NiPs/Ni-foam catalyst. After calcination, $Ni(OH)_2$/Ni-foam converted to NiO/Ni-foam due to thermal decomposition. After reduction, NiPs/Ni-foam exhibited small Ni particles of the size around 2.8 nm, while that NiO/Ni-foam reached as large as 17.7 nm. As a result, compared with NiO/Ni-foam catalyst, NiPs/Ni-foam showed higher catalytic activity for CO_2 methanation with the optimal CO_2 conversion of 70.4% and CH_4 selectivity of 95.5% at 450 °C. The unique combination of Ni-phyllosilicate and Ni-foam over the NiPs/Ni-foam catalyst not only leaded to excellent anti-sintering property, but also provided high heat removal during the CO_2 methanation reaction process, resulting in excellent long-term stability in a 100 h-test.

Supplementary Information The online version contains supplementary material available at https://doi.org/10.1007/s10562-021-03850-y.

Acknowledgements The authors gratefully acknowledge the supports from National Natural Science Foundation of Shandong Province (No. ZR202102220024) and Foundation of Division of Chemical

Sciences of Qingdao University of Science and Technology (No. QUSTHX201912).

Funding This study was funded by Foundation of Division of Chemical Sciences of Qingdao University of Science and Technology (No. QUSTHX201912) and National Natural Science Foundation of Shandong Province (No. ZR202102220024).

Declarations

Conflict of interest The authors declare that they have no conflict of interest.

References

1. Hongmanorom P, Ashok J, Zhang G, Bian Z, Wai MH, Zeng Y et al (2021) Appl Catal B: Environ 282:119564
2. Chen Y, Bi W, Chen L, Liu Q (2021) Int J Hydrogen Energy 46:27567–27575
3. Ye R-P, Gong W, Sun Z, Sheng Q, Shi X, Wang T et al (2019) Energy 188:116059
4. Yang E-H, Kim NY, Noh Y-S, Lim SS, Jung J-S, Lee JS et al (2015) Int J Hydrogen Energy 40:11831–11839
5. Sun J, Li Y, Liu X, Yang Q, Liu J, Sun X et al (2012) Chem Commun 48:3379–3381
6. Sonstrom P, Adam M, Wang X, Wilhelm M, Grathwohl G, Baumer M (2010) J Phys Chem C 114:14224–14232
7. Tomašić V, Jović F (2006) Appl Catal A: Gen 311:112–121
8. Chai R, Li Y, Zhang Q, Zhao G, Liu Y, Lu Y (2016) Mater Lett 171:248–251
9. Shen M, Zhao G, Nie Q, Meng C, Sun W, Si J et al (2021) ACS Appl Mater Inter 13:28334–28347
10. Yuan YF, Xia XH, Wu JB, Yang JL, Chen YB, Guo SY (2011) Electrochim Acta 56:2627–2632
11. Khan Y, Hussain S, Söderlind F, Käll P-O, Abbasi MA, Durrani SK (2012) Mater Lett 69:37–40
12. Lv S, Suo H, Wang J, Wang Y, Zhao C, Xing S (2012) Colloid Surface A 396:292–298
13. Dong H, Liu Q (2020) ACS Sustain Chem Eng 8:6753–6766
14. Zhang T, Liu Q (2020) ACS Appl Mater Inter 12:19587–19600
15. Chen Y, Liu Q (2021) ACS Catal 11:12570–12584
16. White RD, Bavykin DV, Walsh FC (2013) J Mater Chem A 1:548–556
17. Ashok J, Ang ML, Terence PZL, Kawi S (2016) ChemCatChem 8:1308–1318
18. Bian Z, Kawi S (2017) J CO2 Util 18:345–352
19. Li Z, Kawi S (2018) Catal Sci Technol 8:1915–1922
20. Chen Y, Zhang T, Liu Q (2021) Int J Hydrogen Energy 46:30373–30381
21. Zhang C, Yue H, Huang Z, Li S, Wu G, Ma X et al (2012) ACS Sustain Chem Eng 1:161–173
22. Hu B, Qin X, Asiri AM, Alamry KA, Al-Youbi AO, Sun X (2013) Electrochim Acta 107:339–342
23. Yue Z, Yao S, Li Y, Zhu W, Zhang W, Wang R et al (2018) Electrochim Acta 268:211–217
24. Shi M, Cui M, Kang L, Li T, Yun S, Du J et al (2018) Appl Surf Sci 427:678–686
25. Liu Q, Tian Y (2017) Int J Hydrogen Energy 42:12295–12300
26. Yang Y, Liang Q, Li J, Zhuang Y, He Y, Bai B et al (2011) Nano Res 4:882–890
27. Zhang T, Tian Z, Liu Q (2020) Sustain Energy Fuels 4:3438–3449
28. Wang X, Zhu L, Zhuo Y, Zhu Y, Wang S (2019) ACS Sustain Chem Eng 7:14647–14660
29. Li H, Chen Y, Liu S, Liu Q (2021) J CO2 Util 52:101677
30. Bian Z, Kawi S (2020) Catal Today 339:3–23
31. Wang J, Fu Y, Kong W, Jin F, Bai J, Zhang J et al (2021) Appl Catal B: Environ 282:119546
32. Wang T, Liu C, Ma X, Zhu W, Lv X, Zhang H (2019) Nanomaterials 9:998
33. Kim A, Debecker DP, Devred F, Dubois V, Sanchez C, Sassoye C (2018) Appl Catal B: Environ 220:615–625
34. Taherian Z, Khataee A, Orooji Y (2020) Micropor Mesopor Mat 306:110455
35. Zhang Z, Wei T, Chen G, Li C, Dong D, Wu W et al (2019) Fuel 250:176–193
36. Kim M-J, Youn J-R, Kim HJ, Seo MW, Lee D, Go KS et al (2020) Int J Hydrogen Energy 45:24595–24603